Supplement of Atmos. Chem. Phys., 23, 5279–5296, 2023
https://doi.org/10.5194/acp-23-5279-2023-supplement

Atmospheric Chemistry and Physics
Open Access

Supplement of

Revealing the sources and sinks of negative cluster ions in an urban environment through quantitative analysis

Rujing Yin et al.

Correspondence to: Jingkun Jiang (jiangjk@tsinghua.edu.cn)

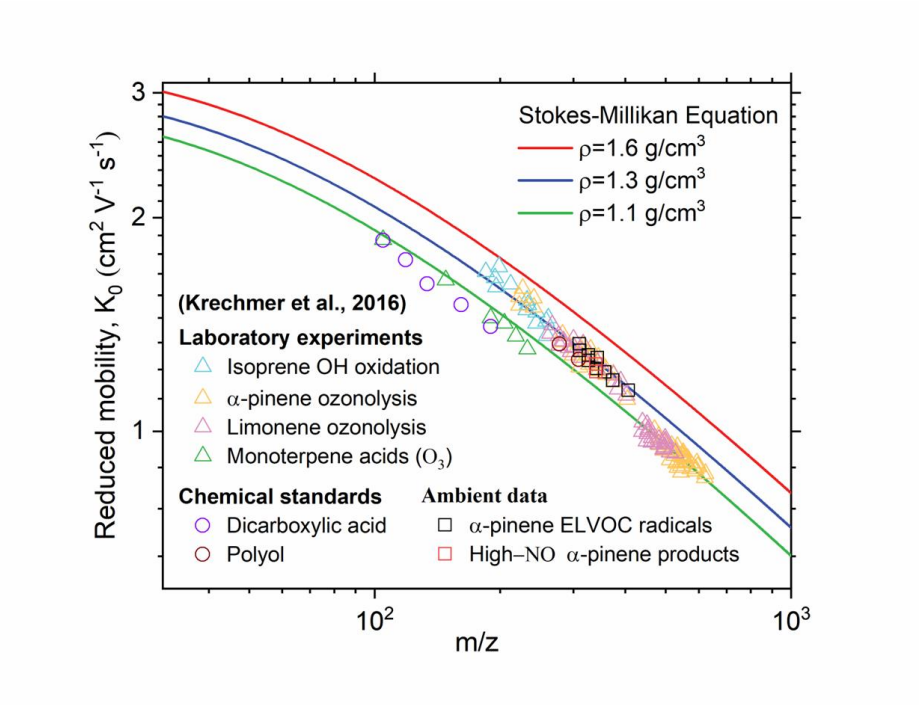

19

20 **Figure S1**. The measured reduced mobilities of different organic cluster ions in ion mobility spectrometer (Krechmer et al.,
21 2016) and simulated mobilities based on the Stokes-Millikan equation using different densities.
22

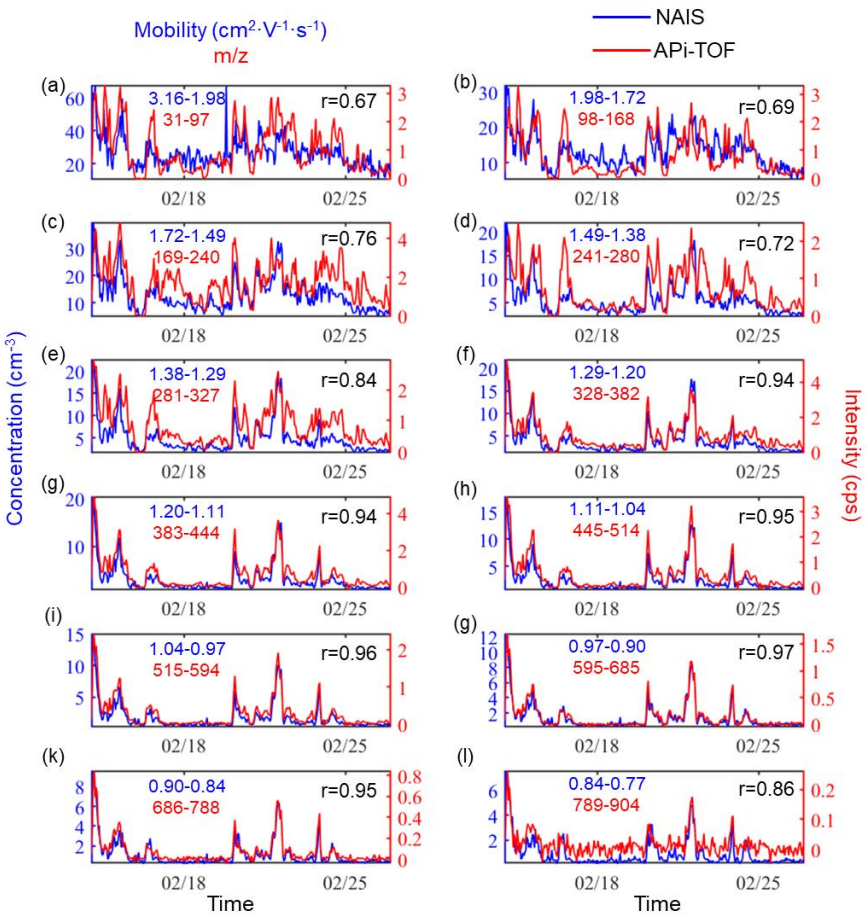

Figure S2. The concentrations of cluster ions with different mobility ranges measured by NAIS and the signal of cluster ions with corresponding *m/z* ranges measured by APi-TOF. The mobility and m/z are converted according to the method described in Section 2.2 in the main text.

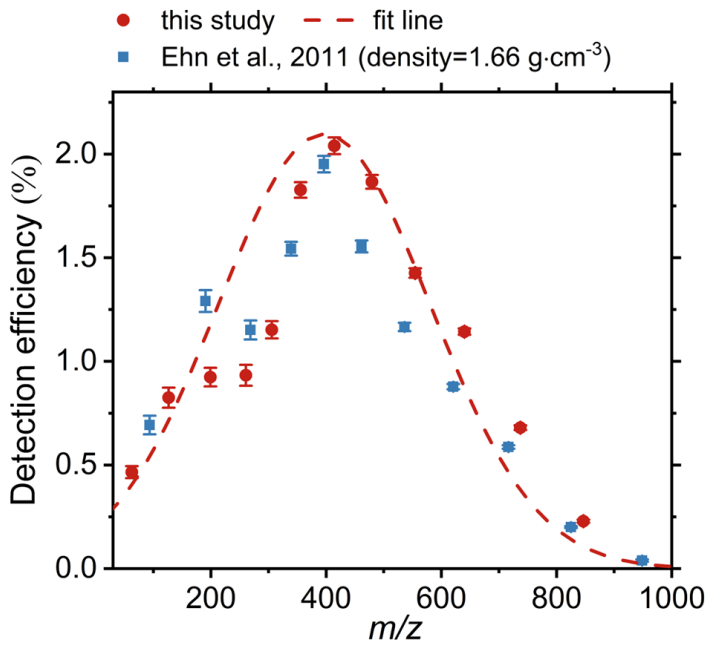

Figure S3. A comparison between the detection efficiency obtained using fixed density (Ehn et al., 2011) and the mass-dependent methods proposed in this study when converting *m/z* to mobility.

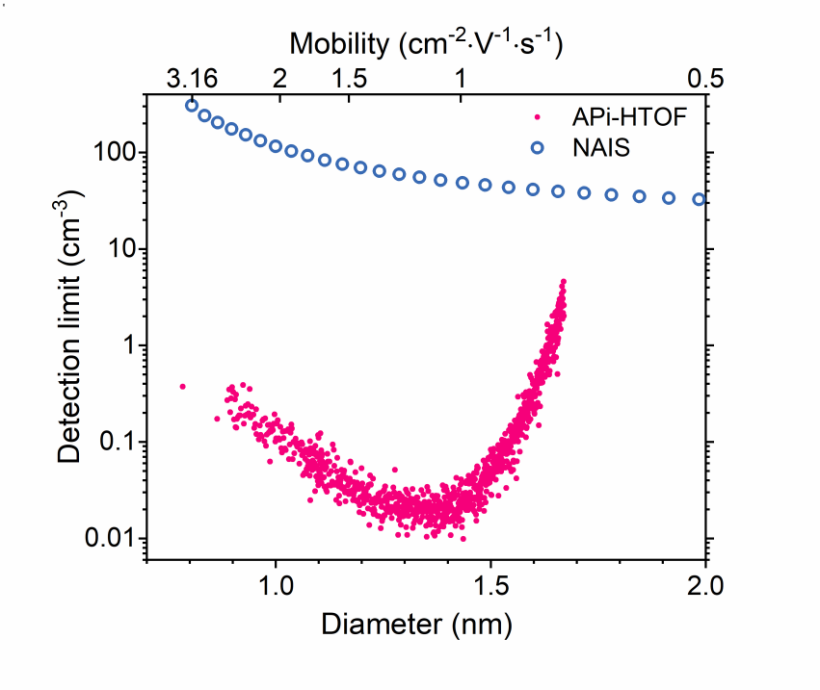

Figure S4. The detection limit of APi-HTOF and NAIS for negative cluster ions. The detection limit of APi-HTOF is determined using data with a resolution of 1 hour, and the detection limit of NAIS is determined using data with a resolution of 2 min. The detection limit of the APi-HTOF is determined according to the noise of microchannel plate (MCP) detector and the detection efficiency. The detection limit of the NAIS is determined according to the noise of the electrometer and its transfer function, and the noise of the electrometer was assumed to be 0.006 fA in this study.

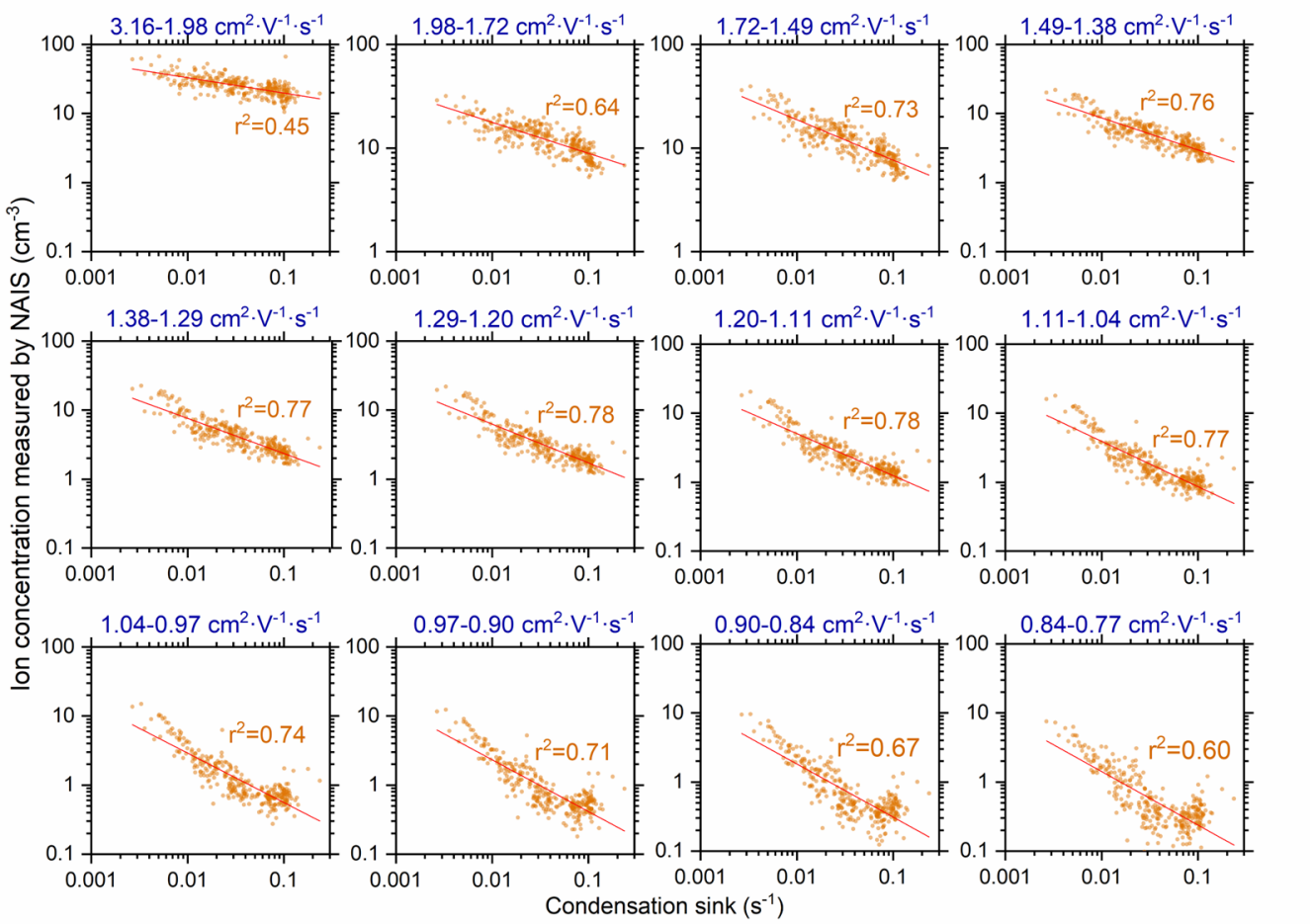

39

40 **Figure S5**. The scatter plots of CS and concentrations of cluster ions with different mobility ranges measured by NAIS in
41 urban Beijing, as well as the square of correlation coefficients.

42

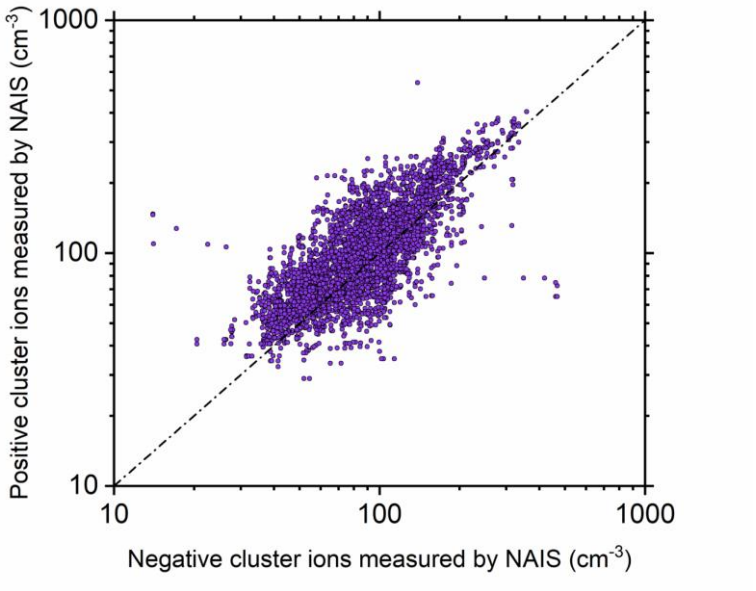

Figure S6. The scatter plots of the concentrations of negative and positive cluster ions measured by NAIS during the measurement in urban Beijing.

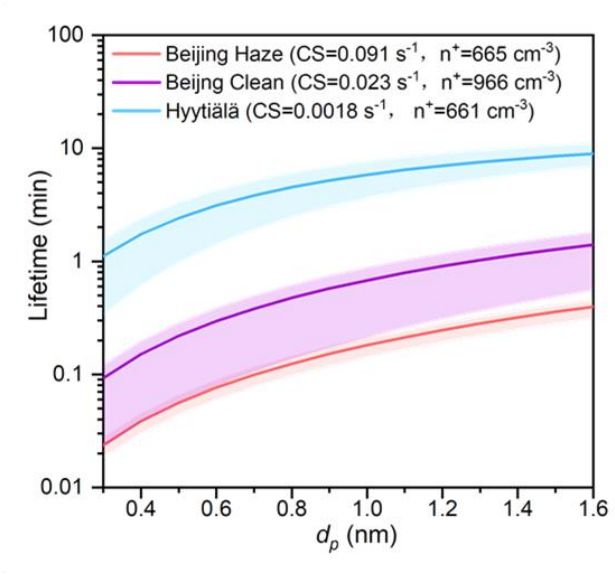

47

48 **Figure S7**. The lifetime (the time needed for the concentration of a given ion concentration to decay to 1/e of its initial
49 value due to the coagulation loss to particles and recombination with opposite ions, calculated as $1/(CS \cdot dp^{-1.7}+\alpha n^{+})$) of
50 the cluster ions under typical conditions (i.e., the median value of CS and median of the total concentration of positive
51 ions in the range of 0.8-42 nm, n^{+}) during haze and clean periods in Beijing and Hyytiälä. The shadow regions represent
52 25-75% of the CS ranges, that is 0.074-0.11 s^{-1}, 0.013-0.034 s^{-1}, and 0.001-0.0023 s^{-1} during Beijing haze periods, Beijing
53 clean periods, and Hyytiälä.
54

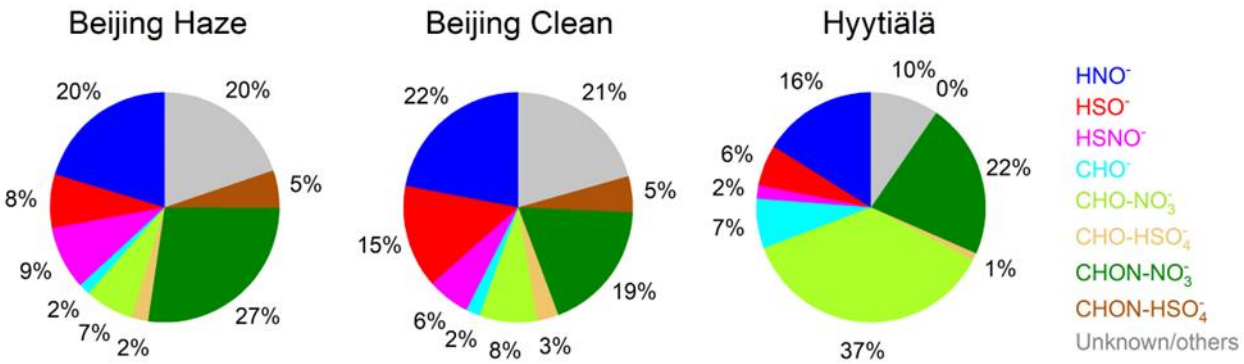

Figure S8. The species distributions of negative cluster ions during haze and clean periods in Beijing and Hyytiälä. Haze periods were identified based on whether $PM_{2.5}$ concentration is higher than 75 $\mu g \cdot m^{-3}$.

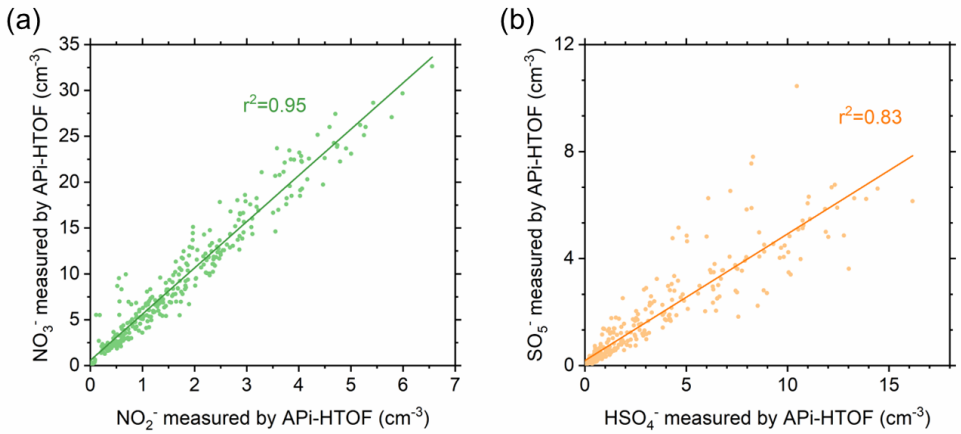

59

60 **Figure S9**. The scatter plot of the concentrations of specific ions measured by APi-TOF in urban Beijing. (a) NO_2^- and NO_3^-;

61 (b) HSO_4^- and SO_5^-.

62

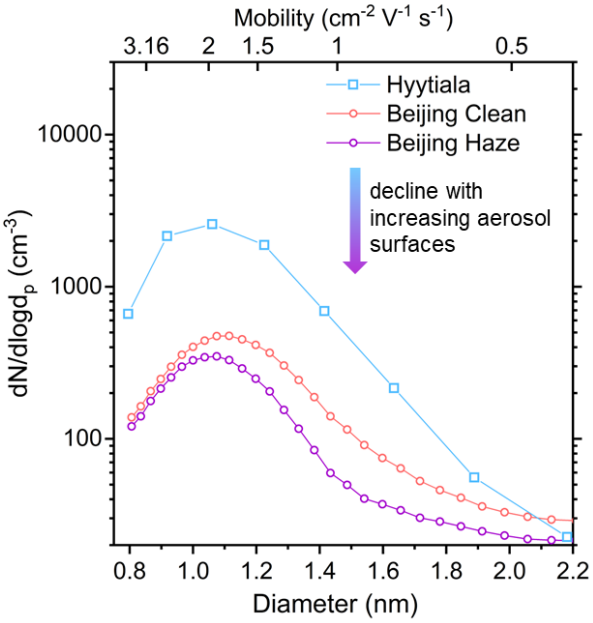

63

64 **Figure S10.** The ion mobility distributions and size distributions measured by NAIS during haze and clean periods in
65 Beijing and Hyytiälä.

66

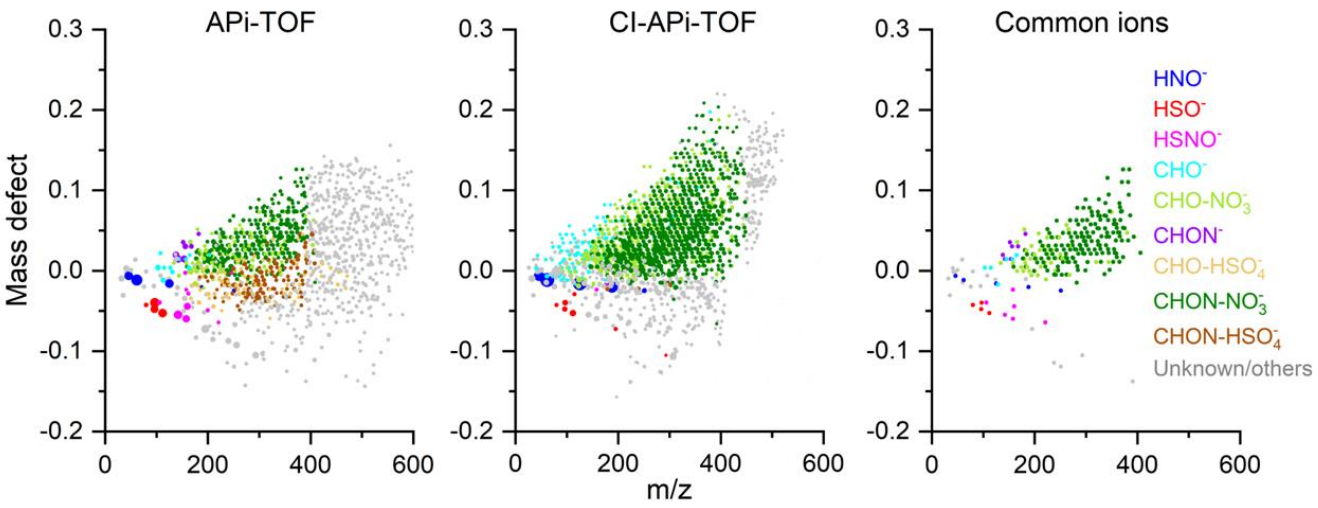

Figure S11. The mass defect plots of the species detected in ions (APi-HTOF), neutral gases (CI-APi-LTOF), and their common species in urban Beijing

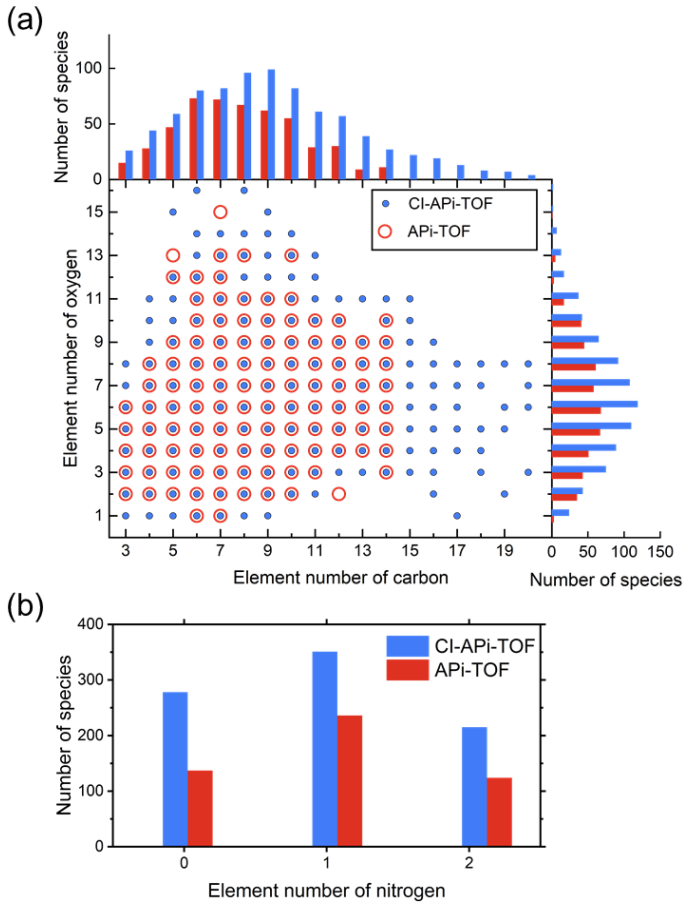

71

72 **Figure S12**. Comparison of the organic molecules detected in APi-TOF and CI-APi-TOF respectively. (a) The distribution of
73 species with different number of carbon atoms and oxygen atoms. (b) The distribution of species with different number of
74 nitrogen atoms.
75

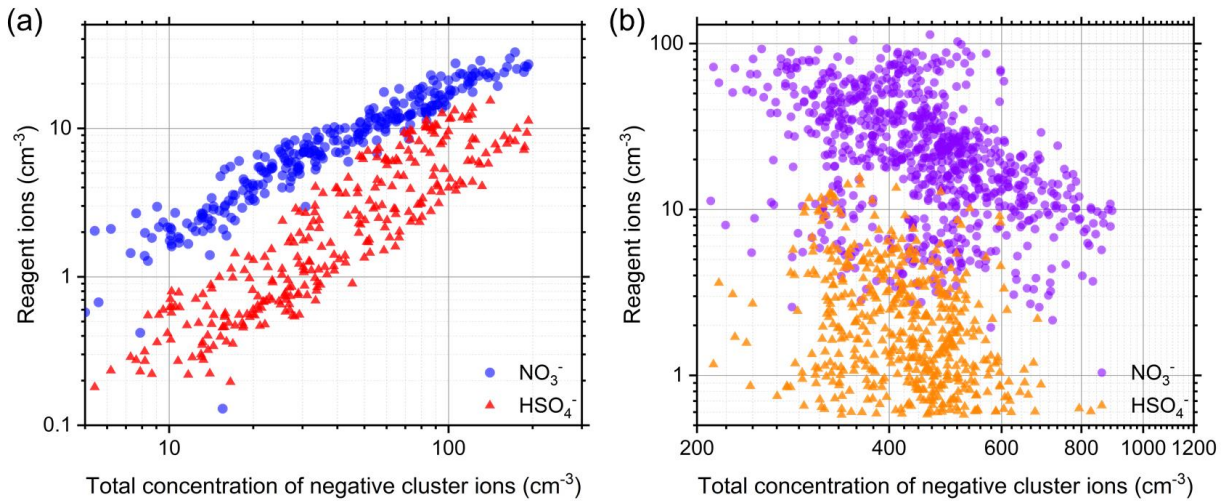

76

77 **Figure S13.** The variation of NO_3^- and HSO_4^- with the total negative cluster ions measured by APi-TOF in (a) urban Beijing

78 and (b) Hyytiälä.

79

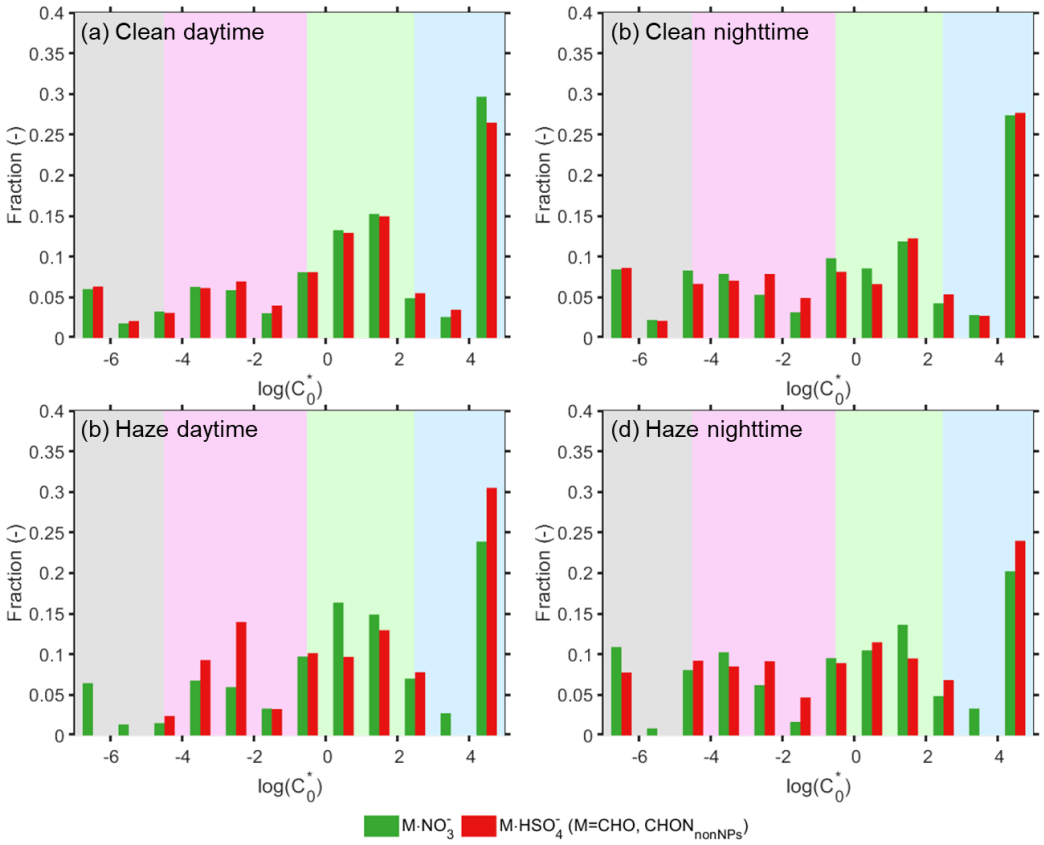

Figure S14. The volatility distribution of CHO and $CHON_{nonNPs}$ species that in the forms of adducts with both NO_3^- and HSO_4^- during different periods and times. (a) Daytime of clean period. (b) Nighttime of clean period. (c) Daytime of haze period. (d) Nighttime of haze period. Only species that attached to both NO_3^- and HSO_4^- were considered for calculating the volatility distribution.

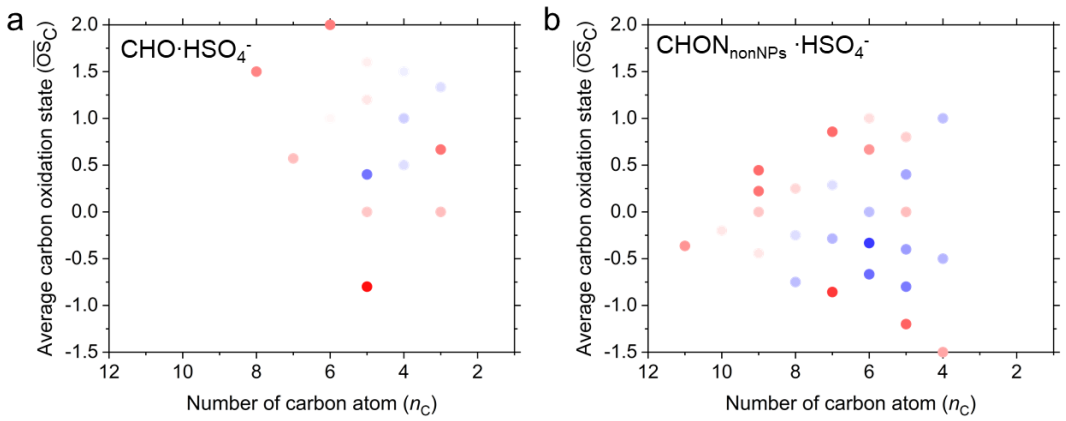

87

88 **Figure S15.** The carbon atom number and average carbon oxidation state ($\overline{OS}_C$) of molecules in $CHO{\cdot}HSO_4^-$ (a) and

89 $CHON_{nonNPs}{\cdot}HSO_4^-$ (b). The color represents their charge fraction during the measurement periods.

90

91

Table S1. The measurement period and time resolution for instruments at AHL/BUCT and SMEAR II stations.

Site, type	Location	Instrument	Time resolution	Measurement period
AHL/BUCT, urban	Beijing, China	APi-HTOF	1 h	Feb 14-Feb 27, 2018
		CI-APi-LTOF	5 min	Jan 23-April 14, 2018
		NAIS	4.5 min	Jan 12-Dec 31, 2018
SMEAR II, boreal forest	Hyytiälä, Finland	APi-HTOF	1 h	April 7-June 8, 2013
		NAIS	4.5 min	Jan 1-Dec 31, 2013

Table S2. The reduced mobilities of NO_3^-, HSO_4^-, and some of their clusters

Formula	m/z	Reduced mobility, K_0 ($cm^{-2}\cdot V^{-1}\cdot s^{-1}$)
O_2^-	31.9904	[a]3.28
NO_2^-	45.9935	[a]2.70
NO_3^-	61.9884	[b]2.45
$HNO_3\cdot NO_3^-$	124.9840	[c]2.07
HSO_4^-	96.9601	[d]2.01
$H_2SO_4\cdot HSO_4^-$	194.9275	[d]1.63
$(H_2SO_4)_2\cdot HSO_4^-$	292.8949	[d]1.27
$(H_2SO_4)_3\cdot HSO_4^-$	390.8622	[d]1.17
$(H_2SO_4)_2\cdot C_2H_7N\cdot HSO_4^-$	337.9527	[d]1.21

[a] From Spangler et al. (Spangler and Collins, 1975)； [b] From Stano et al. (Stano et al., 2008)； [c] From Liang et al. (Liang et al., 2013)； [d] From Jen et al. (Jen et al., 2015)

Reference

Ehn, M., Junninen, H., Schobesberger, S., Manninen, H. E., Franchin, A., Sipila, M., Petaja, T., Kerminen, V. M., Tammet, H., Mirme, A., Mirme, S., Horrak, U., Kulmala, M., and Worsnop, D. R.: An Instrumental Comparison of Mobility and Mass Measurements of Atmospheric Small Ions, Aerosol Sci. Technol., 45, 522-532, 10.1080/02786826.2010.547890, 2011.

Jen, C. N., Hanson, D. R., and McMurry, P. H.: Toward Reconciling Measurements of Atmospherically Relevant Clusters by Chemical Ionization Mass Spectrometry and Mobility Classification/Vapor Condensation, Aerosol Sci. Technol., 49, i-iii, 10.1080/02786826.2014.1002602, 2015.

Krechmer, J. E., Groessl, M., Zhang, X., Junninen, H., Massoli, P., Lambe, A. T., Kimmel, J. R., Cubison, M. J., Graf, S., Lin, Y.-H., Budisulistiorini, S. H., Zhang, H., Surratt, J. D., Knochenmuss, R., Jayne, J. T., Worsnop, D. R., Jimenez, J.-L., and Canagaratna, M. R.: Ion mobility spectrometry–mass spectrometry (IMS–MS) for on- and offline analysis of atmospheric gas and aerosol species, Atmos. Meas. Tech., 9, 3245-3262, 10.5194/amt-9-3245-2016, 2016.

Liang, X., Zhou, Q., Wang, W., Wang, X., Chen, W., Chen, C., Li, Y., Hou, K., Li, J., and Li, H.: Sensitive detection of black powder by a stand-alone ion mobility spectrometer with an embedded titration region, Anal. Chem., 85, 4849-4852, 10.1021/ac400337s, 2013.

Spangler, G. E. and Collins, C. I.: Reactant ions in negative ion plasma chromatography, Anal. Chem., 47, 393-402, 10.1021/ac60353a019, 1975.

Stano, M., Safonov, E., Kucera, M., and Matejcik, S.: Ion Mobility Spectrometry Study of Negative Corona Discharge in Oxygen/Nitrogen Mixtures, Chem. Listy, 102, S1414-S1417, 2008.